Design and stability of NOR and NAND logic gates constructed with three quantum states

N. Renaud and C. Joachim*
Nanoscience Group, CEMES/CNRS, 29 rue J. Marvig, BP 94347, 31055 Toulouse Cedex, France
(Received 2 July 2008; published 8 December 2008)

By encoding the digital input of a classical logic gate on the Hamiltonian of a quantum system and driving the logic operation by preparing it in the same nonstationary state whatever the input, NOR and NAND classical logic gates are designed with a minimum of three quantum states. The outputs of one gate are obtained either by measuring the distance between the $\rho(t)$ periodic quantum trajectory and the output target state ρ_b, or by measuring the secular frequency of the $\rho(t)$ almost periodic trajectory in the ρ_b direction. A comparison of the stability to noise between the two approaches demonstrates that the frequency approach is more immune to random fluctuations in the Hamiltonian than a distance control approach, opening the way to determine the logic output using a tunneling current passing through the gate.

DOI: 10.1103/PhysRevA.78.062316 PACS number(s): 03.67.Lx, 73.63.−b

I. INTRODUCTION

When an isolated quantum system is prepared in a nonstationary state $\rho(0)$, its resulting intrinsic quantum evolution can be used to drive a digital logic operation [1–6]. The design of the corresponding Hamiltonian $\mathcal{H}$ depends on the way to input the data and to measure the result of the logic operation. A well-known solution for encoding the $\{\ldots,\alpha_i,\ldots\}$ digital inputs on the quantum system is to prepare a $|\Psi(0)\rangle=|\ldots,\alpha_i,\ldots\rangle$ initial state vector with $\rho(0)=|\ldots,\alpha_i,\ldots\rangle\langle\ldots,\alpha_i,\ldots|$. Since the $\rho(t)$ quantum trajectory on the phase space is controlled by $\mathcal{H}$ according to $\rho(t)=e^{i\mathcal{H}t/\hbar}\rho(0)e^{-i\mathcal{H}t/\hbar}$, other ways to input and output data on a quantum system are possible. For example, the input data can be encoded on the Hamiltonian that is $\mathcal{H}=\mathcal{H}(\ldots,\alpha_i,\ldots)$ as proposed in the so-called quantum Hamiltonian computer approach (QHC) [2,7,8]. Recently, this encoding was used to optimize the chemical structure of a molecule 1/2 digital adder [9]. Furthermore, instead of tracking the output by measuring the distance between $\rho(t)$ and a given output target state ρ_b, one can measure the main oscillation frequency between $\rho(t)$ and ρ_b, that is the dominant frequency in the Fourier spectrum of the $\mathrm{Tr}[\rho(t)\rho_b]$ function. This QHC solution opens a way of designing monomolecular logic gate [9] since this frequency is closely related to the tunneling current intensity through a quantum system, for example, a single molecule interconnected to metallic pads [10].

In this paper and for a 2 inputs (α,β)-one output classical logic gate running quantum mechanically, the stability of a $\rho(t)$ distance control versus a $\rho(t)$ frequency control is studied with the prospect of designing efficient quantum logic gates by encoding the input on a Hamiltonian defined by a minimum number of quantum states. As compared to a qubit logic gate approach, this encoding is more suitable for embedding a logic gate on a single molecule performing alone a classical logic operation [9]. In Sec. II, the general characteristic of a $\rho(t)$ distance and frequency control on a quantum state space are recalled defining the output measurement for both cases. In Secs. III and IV and using a three quantum states system, we, respectively, present the design of a distance controlled NOR gate and a frequency controlled NAND gate. Those two different gates have been chosen because they can be implemented using the same Hamiltonian and with a minimum of three quantum states which is a very important constraint in the prospect of limiting the complexity of the molecule which will carry such computing states. It can also be shown that those two gates cannot be implemented in a two quantum states system using the same QHC approach. In Sec. V, the stability of this QHC approach to noise is discussed, showing a better noise immunity for a frequency control. Extensions of this work are discussed in the conclusion.

II. TRAJECTORY CONTROL OF $\rho(t)$ IN ITS QUANTUM STATES SPACE

After its initial preparation in a state $\rho(0)=\rho_a$, $\rho(t)$ describes the intrinsic time evolution of a quantum system whose evolution can be controlled by a well identified set of two parameters $\{\alpha,\beta\}$ of its $\mathcal{H}(\alpha,\beta)$ Hamiltonian. In a QHC approach and whatever the $\{\alpha,\beta\}$ values, this quantum system must be prepared in the same physical initial state ρ_a called the driving state even if the decomposition of the corresponding $|\phi_a\rangle$ on the $\mathcal{H}(\alpha,\beta)$ eigenbasis set is modified according to the Hamiltonian input parameters change. To fully appreciate how this control is performed, $\rho(t)$ can be represented by the motion of a point circulating in the so-called quantum state space ϵ [11–13]. In the following sections and in a way to simplify this geometrical representation, $\rho(t)$ will be presented as resulting from the quantum evolution of a $(N=2)$-states quantum system: $\rho_2(t)=P_{|\phi_a\rangle|\phi_b\rangle}\rho(t)P_{|\phi_a\rangle|\phi_b\rangle}$, where $P_{|\phi_a\rangle,|\phi_b\rangle}$ is the projector on the subspace generated by $|\phi_a\rangle$ and $|\phi_b\rangle$ with $|\phi_b\rangle$ the target state vector. With this projection, $\rho(t)$ can be represented by the motion of a point on the so-called Bloch sphere in R^3 [13]. In Secs. III and IV, this reduced trajectory is used to figure out how $\rho(t)$ is controlled in ϵ by the logic input of the NOR and NAND QHC logic gates. Notice that after this projection and since $\mathrm{Tr}[\rho_2(t)]$ is not *a priori* equal to unity, the corresponding trajectory may enter the interior of the Bloch sphere at

*joachim@cemes.fr

some time and collapse at its center. Hereafter and starting from the same initial state ρ_a, we are considering two types of trajectory control: A distance control between $\rho(t)$ and a given target state and a frequency control which consists of controlling the $\rho(t)$ dominant oscillation frequency in the direction of ρ_b.

When running a logic gate of the Boolean equation $\mathfrak{B}(\alpha,\beta)$ [14] by a distance control in a QHC approach, the output logic "1" is attributed to a zero distance and the "0" logic to the maximum possible distance on ϵ between $\rho(t)$ and ρ_b that is $D(\rho(t),\rho_b)=1-\mathfrak{B}(\alpha,\beta)$ with by definition $D(\rho(t),\rho_b)=\frac{1}{2}\mathrm{Tr}\{[\rho(t)-\rho_b]^2\}$ the normalized to unity Hilbert-Schmidt distance on ϵ. When $\rho(t)$ and ρ_b are pure states and using a projective measurement, this distance simply reduces to $D(\rho(t),\rho_b)=1-\mathrm{Tr}[\rho(t)\rho_b]$ with

$$\mathrm{Tr}[\rho(t)\rho_b]=\sum_{n=1}^{N}c_n^2i_n^2+2\sum_{n=1}^{N-1}\sum_{m>n}^{N}c_ni_nc_mi_m\cos(w_{mn}t). \quad (1)$$

In Eq. (1), i_n and c_n are, respectively, the coefficients of the development of $|\phi_a\rangle$ and $|\phi_b\rangle$ on the $\mathcal{H}$ eigenbasis, with the restriction c_n, $i_n\in\mathbb{R}$. The ω_{mn} are given by the differences between any two $\mathcal{H}$ eigenvalues λ_n and λ_m. For $D(\rho(t),\rho_b)$ to equal exactly zero or one, three conditions must be respected. The first one is to get a fully periodic trajectory on ϵ. To satisfy this condition, all the $\mathcal{H}$ eigenvalues, which are depending on the $\{\ldots,\alpha_i,\ldots\}$ inputs, must be commensurable with each other, i.e., $\lambda_k=\mathcal{R}z_k$ with $\mathcal{R}\in\mathbb{R}$ and $z_k\in\mathbb{Z}$. Then to reach ρ_b, the coefficients c_n and i_n must also satisfy two other conditions: $|c_n|=|i_n|$ for all n and $c_ni_nc_mi_m>0$ (respectively, $c_ni_nc_mi_m<0$) if z_m-z_n is even (respectively, odd) [15].

When all of those are fulfilled, the distance between $\rho(t)$ and ρ_b can reach zero, or its maximum value, only at time $\tau_m=\frac{\tau}{2}+m\tau$, where τ is the period of the trajectory [15].

Consequently, for a distance controlled QHC logic gate, the outcome of the gate will only be accessible exactly at the time series τ_m, since it is only at those times that the distance can reach zero or one. This outcome can be obtained by a projective measurement on ϵ, that is, by measuring the population of the corresponding $|\phi_b\rangle$ for a pure state.

To build the corresponding $\mathcal{H}$ for driving a periodic $\rho(t)$, we propose to study first the properties of the evolution operator $\mathcal{U}(t)=e^{-i\mathcal{H}t/\hbar}$, since once $\mathcal{U}(t)$ is properly constructed, $\mathcal{H}$ can be calculated using the relation

$$\mathcal{H}=\frac{i\hbar}{t}\ln\mathcal{U}(t). \quad (2)$$

Since only periodic trajectories with a period τ are of interest here, the Lie group defined by the $\mathcal{U}(t)$ operators can be reduced to the operators $\mathcal{U}(0<t<\tau)$ with $\mathcal{U}(\tau)=\mathcal{U}(0)=\mathbb{I}$ [16]. Besides, since the trajectory reaches the target state only at $\tau_m=\frac{\tau}{2}+m\tau$, no pertinent information on the evolution in time are lost by considering only a subgroup of the Lie group, containing $\mathcal{C}$ elements, with among them $\mathbb{I}$ and $\mathcal{U}(\tau/2)$. In this case, the continuous Lie group becomes a cyclic group [17] whose generator is $\mathcal{U}_g=e^{-i\mathcal{H}(\tau/\hbar\mathcal{C})}$. The cardinal of the cyclic group $\mathcal{C}$ controls the discretization of the Lie group into the cyclic group and can be set at wish as long as it remains even with $\mathcal{C}>2\max(\ldots,k_n,\ldots)$ in order to ensure that the cyclic group contains $\mathcal{U}(\tau/2)$. Each eigenvalue of the generator belong to the group of the $\mathcal{C}$th roots of $\mathbb{I}$, since $\mathcal{U}_g=\sqrt[\mathcal{C}]{\mathbb{I}}$, and can be written $e^{2ik_n(\pi/\mathcal{C})}$ with a different $k_n\in\mathbb{Z}$ per eigenvalue. The generator of the group is given by $\mathcal{U}_g=\mathcal{P}\mathcal{S}_{\mathcal{U}_g}\mathcal{P}^\dagger$ with $\mathcal{P}$ the matrix to pass from the canonical basis to the eigenbasis of the logic gate Hamiltonian and $\mathcal{S}_{\mathcal{U}_g}$ the diagonal form of $\mathcal{U}_g$. Then, for a periodic trajectory of period τ, $\mathcal{H}$ is given, applying (2) at time τ_g, by

$$\mathcal{H}=\frac{i\hbar}{\tau_g}\ln[\mathcal{U}(\tau_g)]=i\hbar\frac{\mathcal{C}}{\tau}\mathcal{P}\ln(S_{\mathcal{U}_g})\mathcal{P}^\dagger. \quad (3)$$

In Eq. (3), the $\mathcal{C}$ parameter does not affect the $\mathcal{H}$ matrix elements because $S_{\mathcal{U}_g}$ depending on $\mathcal{C}$, $\ln(S_{\mathcal{U}_g})$ eliminate the $\mathcal{C}$ dependency in (3). At the measuring time series τ_m and when $\rho(t)$ is driven by (3), $D(\rho(\tau_m),\rho_b)$ is simply related to $\mathcal{U}_g$ by

$$\begin{aligned}D(\rho(\tau_m),\rho_b)&=1-|\langle\phi_b|e^{-i\mathcal{H}(\tau/2\hbar)}|\phi_a\rangle|^2\\&=1-|\langle\phi_b|(\mathcal{U}_g)^{\mathcal{C}/2}|\phi_a\rangle|^2. \quad (4)\end{aligned}$$

Controlling this distance as a function of the $\{\alpha,\beta\}$ input parameters is the key of the logic gate design in a distance control approach. Those inputs control the trajectory deformation in order for $\rho(t)$ either to reach ρ_b or to belong to the ρ_b orthogonal subspace at the measuring time.

When running now a logic gate using a frequency control in the QHC approach, the output logic is set to "1" when the secular oscillation frequency Ω, defined as the dominant component of the Fourier transform of $\mathrm{Tr}[\rho(t)\rho_b]$, is large, for example, a few petahertz (PHz) in the case of an intramolecular electron transfer process. On the contrary, when Ω is a low frequency, i.e., a few terahertz (THz) or less, the output of the logic function is considered to be the "0" logic. The relation between Ω and the Boolean equation $\mathfrak{B}(\alpha,\beta)$ is simply $\Omega(\alpha,\beta)=k\mathfrak{B}(\alpha,\beta)$ with k as a structural parameter independent of the $\{\alpha,\beta\}$ inputs [18,19]. This encoding opens the way to a determination of the gate outcome by measuring the tunneling current intensity passing through the logic gate because in first approximation, this intensity is proportional to the square of the $\rho(t)$ secular oscillation frequency Ω [10]. With such a frequency controlled logic gate, there is no need for a periodic $\rho(t)$ evolution nor for the $\rho(t)$ trajectory to pass exactly by the outcome target state, since the only important parameter is Ω. Here, the trajectory control seems easier than a distance control for operating the gate. This is at the expense of the fact that measuring Ω with the tunneling current intensity will increase the running time of the gate due to its electronic interactions with contacting metallic pads [10].

The secular frequency Ω is usually obtained by constructing a 2-states effective Hamiltonian, $\mathcal{H}_{\mathrm{eff}}$, using the two eigenstates of the total Hamiltonian as close as possible to Hilbert subspace generated by $|\phi_a\rangle$ and $|\phi_b\rangle$ [18]. This procedure is equivalent to filter the time dependent $\mathrm{Tr}[\rho(t)\rho_b]$ function entering in the calculation of $D(\rho(t),\rho_b)$ in a way to define, from $|\phi_a\rangle$ and $|\phi_b\rangle$, a model 2-states Rabi-like quantum system.

The secular frequency $\Omega=w_{kl}$ governing the secular oscillation amplitude (1), is given by the couple (k,l) maximizing

$c_n i_n c_m i_m$. Identifying this couple leads to a simple Rabi-like oscillation fitting the oscillations in (1) by the simple expression [18]

$$\mathrm{Tr}[\rho(t)\rho_b] = A \sin^2\left(\frac{\Omega}{2}t\right) \tag{5}$$

with $A=(\Sigma_{n=1}^{N}|c_n||i_n|)^2$ and the corresponding effective Hamiltonian given by

$$\mathcal{H}_{\mathrm{eff}} = \begin{pmatrix} 0 & \frac{\sqrt{A}\Omega}{2} \\ \frac{\sqrt{A}\Omega}{2} & \Omega\sqrt{1-A} \end{pmatrix} \tag{6}$$

Controlling Ω as a a function of the $\{\alpha,\beta\}$ input parameters is the basis of the frequency control implementation. A change in the input configuration must induce a acceleration or deceleration of $\rho(t)$ in the ρ_b direction on ε.

When running a QHC logic gate in a distance or frequency control, the Hamiltonian $\mathcal{H}(\alpha,\beta)$ gives rise to four Hamiltonians, $\mathcal{H}_{\alpha\beta}$, one for each (α,β) input configuration. To build a logic gate respecting a given truth table, the properties of each $\rho_{\alpha\beta}(t)$ generated by $\mathcal{H}_{\alpha\beta}$ will be first studied separately in the following using either the cyclic group approach to control $D(\rho_{\alpha\beta}(t),\rho_b)$ or the effective Hamiltonian approach to control $\Omega_{\alpha\beta}$ as discussed above. In a second step, the four constructed $\mathcal{H}_{\alpha\beta}$ are unified in a final $\mathcal{H}(\alpha,\beta)$ Hamiltonian, identifying the values of the structural parameters, i.e., the matrix element which are identical for all the α and β values.

To evaluate the performance and the stability to external perturbations of our QHC gates, the Gaussian function

$$\mathcal{F} = \prod_{i,j} e^{-[(\mathcal{M}_{\alpha\beta}-\mathcal{I}_{\alpha\beta})^2/2\sigma^2]} \tag{7}$$

will be used as a measurement of the gate fidelity, i.e., how close the gate is to its expected logic truth table. In (7), $\mathcal{I}_{\alpha\beta}$ and $\mathcal{M}_{\alpha\beta}$ are, respectively, the ideal output of the expected logic gate and the result obtained with the designed logic gate both for the (α,β) input configuration. The σ parameter can be tuned to change the sharpness of the fidelity function. $\sigma=\frac{1}{4}$ gives a sharp $\mathcal{F}$ function and will be used in the following. For a distance control and since the distance between $\rho(t)$ and a target state ranges between zero and one because of $D(\rho(t),\rho_b)=1-\mathfrak{B}(\alpha,\beta)$, the resulting $\mathcal{M}_{\alpha,\beta}$, used to calculate (7) is given by $\mathcal{M}_{\alpha\beta}=1-D(\rho_{\alpha\beta}(\tau_m),\rho_b)$. For a frequency control, the secular oscillation frequency $\Omega_{\alpha\beta}$ of a given trajectory do not range between zero and one. In this case, the $\Omega_{\alpha\beta}$ are normalized in reference to the maximum secular oscillation frequency leading to $\mathcal{M}_{\alpha\beta}=\frac{\Omega_{\alpha\beta}}{\max\{\cdots\Omega_{\alpha'\beta'\cdots}\}}$ as used in (7).

In the following, those definitions and tools will be applied to the 3-states quantum system presented in Fig. 1 where α and β are the two input parameters of the logic gate. On the corresponding $|\phi_a\rangle$, $|\phi_b\rangle$, and $|\phi_e\rangle$ canonical basis set, the general form of our Hamiltonian is

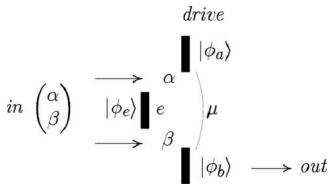

FIG. 1. The 3-state system chosen to embody the NOR and the NAND gates. The two parameters α and β are used to encode the input information, e and μ being the structural parameters of the gate. The system is initially prepared in the $\rho_a=|\phi_a\rangle\langle\phi_a|$ state and the output is either in the distance between $\rho(t)=|\psi(t)\rangle\langle\psi(t)|$ and the target state $\rho_b=|\phi_b\rangle\langle\phi_b|$ or in the secular oscillation frequency of $\rho(t)$ in the direction of ρ_b.

$$\mathcal{H}(\alpha,\beta) = \begin{pmatrix} 0 & \mu & \alpha \\ \mu & 0 & \beta \\ \alpha & \beta & e \end{pmatrix}, \tag{8}$$

where $|\phi_e\rangle$ is a structural state. Depending on the value of the structural parameters e and μ, a NOR gate can be obtained in a distance control approach and a NAND gate in a rate control approach. For convenience, all the parameters will be normalized for α and β to take only the values 0.0 or 1.0 eV. This 3-states quantum system is prepared in the ρ_a initial state to provide the energy to run the gate and ρ_b is the output state. Notice that with (8), the $|\phi_b\rangle$ occupation probability is given by a relatively simple analytical expression for $\alpha=\beta$, i.e., for the $(\alpha,\beta)=(0,0)$ or (1,1) logic configurations:

$$\begin{aligned}\mathrm{Tr}[\rho(t)\rho_b] = 1/4[1 &+ \cos^4(\theta) + \sin^4(\theta) \\ &+ 2\cos^2(\theta)\sin^2(\theta)\cos(\Omega_0 t) - 2\sin^2(\theta)\cos(\Omega_+ t) \\ &- 2\cos^2(\theta)\cos(\Omega_- t)],\end{aligned} \tag{9}$$

with

$$\Omega_0 = \sqrt{(e-\mu)^2+8\alpha^2}, \quad \Omega_\pm = \frac{e+3\mu}{2} \pm \frac{\Omega_0}{2},$$

$$\text{and } \cos(\theta) = \sqrt{\frac{\Omega_+ - 2\mu}{\Omega_0}}. \tag{10}$$

Even for this $\alpha=\beta$ symmetric case and as discussed in the two next sections, it is difficult to find analytically the good e and μ values in (8) for $\mathrm{Tr}[\rho(t)\rho_b]$ to reach $\mathfrak{B}(\alpha,\beta)=\alpha+\beta$ periodically in time for a distance controlled NOR gate or for Ω to be proportional to $\mathfrak{B}(\alpha,\beta)=\alpha\cdot\beta$ for a frequency controlled NAND gate. The design of those two gates is discussed in the next two sections.

III. DESIGN OF A NOR GATE IN A DISTANCE CONTROL APPROACH

For the Hamiltonian (8) to drive a distance controlled NOR logic gate in time, the distance between $\rho(t)$ and the output target state ρ_b must verify $D(\rho(t),\rho_b)=1-\alpha+\beta$ at periodic intervals τ. According to (3), each of the four $\mathcal{H}_{\alpha\beta}$ is defined by

$$\mathcal{H}_{\alpha\beta} = i\hbar \frac{\mathcal{C}_{\alpha\beta}}{\tau} \mathcal{P}_{\alpha\beta} \ln(S_{\mathcal{U}_{g,\alpha\beta}}) \mathcal{P}^{\dagger}_{\alpha\beta}. \tag{11}$$

Since for $\alpha \neq \beta$ there is no simple analytical solution to the time-dependent Schrödinger equation leading to $\rho(t)$, we apply first the cyclic group approach to $\alpha=\beta$. Then, the $\alpha \neq \beta$ cases will be deduced starting from the $\alpha=\beta$ case by a numerical optimization. For $\alpha=\beta$, the $\mathcal{P}(\theta_{\alpha\alpha})$ matrix to pass from the canonical basis set to the $\mathcal{H}_{\alpha\alpha}$ eigenbasis set is simply an SO(3) rotation matrix of angle $\theta_{\alpha\alpha}$,

$$\mathcal{P}(\theta_{\alpha\alpha}) = \frac{1}{\sqrt{2}} \begin{pmatrix} \cos(\theta_{\alpha\alpha}) & 1 & \sin(\theta_{\alpha\alpha}) \\ \cos(\theta_{\alpha\alpha}) & -1 & \sin(\theta_{\alpha\alpha}) \\ \sqrt{2}\sin(\theta_{\alpha\alpha}) & 0 & -\sqrt{2}\cos(\theta_{\alpha\alpha}) \end{pmatrix}. \tag{12}$$

The three $\mathcal{U}_{g,\alpha\alpha}$ eigenvalues required to calculate $\mathcal{H}_{\alpha\alpha}$ using (3) are $e^{2ik_1^{\alpha\alpha}(\pi/\mathcal{C}_{\alpha\alpha})}$, $e^{2ik_2^{\alpha\alpha}(\pi/\mathcal{C}_{\alpha\alpha})}$, and $e^{2ik_3^{\alpha\alpha}(\pi/\mathcal{C}_{\alpha\alpha})}$ where $k_1^{\alpha\alpha}$, $k_2^{\alpha\alpha}$, and $k_3^{\alpha\alpha} \in \mathbb{Z}$. The analytical expression of $\mathcal{H}_{00}$ and $\mathcal{H}_{11}$ is needed for those two Hamiltonians to have identical structural parameters. Those expressions have been calculated from (11) using $\theta_{\alpha\alpha}=0$ for $\alpha=0$ and $\theta_{\alpha\alpha}=\theta$ for $\alpha=1$. This leads to

$$\mathcal{H}_{00} = -\frac{\hbar\pi}{\tau} \begin{pmatrix} 0 & k_1^{00}-k_2^{00} & 0 \\ k_1^{00}+k_2^{00} & 0 & 0 \\ 0 & 0 & k_3^{00}-(k_1^{00}+k_2^{00}) \end{pmatrix}, \tag{13}$$

$$\mathcal{H}_{11}(\theta) = -\frac{\hbar\pi}{\tau} \begin{pmatrix} 0 & k_3^{11}\sin(\theta)^2 + k_1^{11}\cos(\theta)^2 - k_2^{11} & \kappa(k_n^{11},\theta) \\ k_3^{11}\sin(\theta)^2 + k_1^{11}\cos(\theta)^2 - k_2^{11} & 0 & \kappa(k_n^{11},\theta) \\ \kappa(k_n^{11},\theta) & \kappa(k_n^{11},\theta) & f(k_n^{11},\theta) \end{pmatrix} \tag{14}$$

with $\kappa(k_n^{11},\theta)=\sqrt{2}(k_3^{11}-k_1^{11})\cos(\theta)\sin(\theta)$ and $f(k_n^{11},\theta) = \sin^2(\theta)(2k_1^{11}-k_3^{11}) + \cos^2(\theta)(2k_3^{11}-k_1^{11}) - k_2^{11}$. Note that for $\mathcal{H}_{00}$ and $\mathcal{H}_{11}$ to originate from (8) one needs to set $\langle\phi_a|\mathcal{H}_{\alpha\alpha}|\phi_a\rangle = \langle\phi_b|\mathcal{H}_{\alpha\alpha}|\phi_b\rangle = 0$. This is not the case using the cyclic generator $\mathcal{H}_{\alpha\alpha}$ analytical expression above. Therefore, to ease the calculation, we have shifted the $\mathcal{H}_{\alpha\alpha}$ diagonal elements, $\mathcal{H}_{\alpha\alpha} = \mathcal{H}_{\alpha\alpha} - \mathbb{I}\langle\phi_a|\mathcal{H}_{\alpha\alpha}|\phi_a\rangle$, because this shift does not modify the evolution generated by $\mathcal{H}_{\alpha\alpha}$. Furthermore, the time evolution driven by $\mathcal{H}_{00}$ belongs only to the subspace generated by $|\phi_a\rangle$ and $|\phi_b\rangle$. Then, a change in the $\langle\phi_e|\mathcal{H}_{00}|\phi_e\rangle$ matrix element value does not induce a deformation of the corresponding trajectory. Consequently, μ is the only structural parameter identical in $\mathcal{H}_{00}$ and $\mathcal{H}_{11}$. Identifying the two μ values in (13) and (14) leads to the equation

$$k_1^{00} - k_2^{00} = k_3^{11}\sin(\theta)^2 + k_1^{11}\cos(\theta)^2 - k_2^{11} \tag{15}$$

whose solution leads to the angle θ series

$$\cos(\theta) = \pm \sqrt{\frac{k_1^{00} - k_2^{00} + k_2^{11} - k_3^{11}}{k_1^{11} - k_3^{11}}}. \tag{16}$$

Using only those θ in (13) and (14), the two Hamiltonians present compatible structural parameters. Now all the $\mathcal{H}(\alpha,\beta)$ matrix elements are normalized by $\frac{\hbar\pi}{\tau}\kappa(k_n^{11},\theta)$ for α and β to take only the values 0.0 or 1.0 eV. The structural parameters e and μ read as

$$\mu = \frac{k_3^{11}\sin(\theta)^2 + k_1^{11}\cos(\theta)^2 - k_2^{11}}{\sqrt{2}(k_3^{11}-k_1^{11})\cos(\theta)\sin(\theta)}, \tag{17}$$

$$e = \frac{k_1^{11}[2\sin^2(\theta) - \cos^2(\theta)] + k_3^{11}[2\cos^2(\theta) - \sin^2(\theta)] - k_2^{11}}{\sqrt{2}(k_3^{11}-k_1^{11})\cos(\theta)\sin(\theta)}. \tag{18}$$

Using (4) the relation between $D(\rho_{\alpha\alpha}(\tau_m),\rho_b) = 1 - \mathrm{Tr}[\rho_{\alpha\alpha}(\tau_m)\rho_b]$ and the $k_1^{\alpha\alpha}, k_2^{\alpha\alpha}, k_3^{\alpha\alpha}$ parameters is simply given by

$$D(\rho_{\alpha\alpha}(\tau_m),\rho_b) = 1 - \tfrac{1}{4}|\cos^2(\theta)e^{ik_1^{\alpha\alpha}\pi} + \sin^2(\theta)e^{ik_3^{\alpha\alpha}\pi} - e^{ik_2^{\alpha\alpha}\pi}|^2. \tag{19}$$

The control of the $\{k_1^{\alpha\alpha}, k_2^{\alpha\alpha}, k_3^{\alpha\alpha}\}$ parameters on $D(\rho_{\alpha\alpha}(\tau_m),\rho_b)$ is now obvious, $D(\rho_{\alpha\alpha}(\tau_m),\rho_b)=0$ when $(k_1^{\alpha\alpha}, k_3^{\alpha\alpha})$ and $k_2^{\alpha\alpha}$ are of different parity and $D(\rho_{\alpha\alpha}(\tau_m),\rho_b)=1$ when the three different $k_n^{\alpha\alpha}$ are of the same parity. Imposing those parity conditions, the truth table of a NOR gate is exactly fulfilled for $\alpha=\beta$ with as required $D(\rho_{00}(\tau_m),\rho_b)=0$ and $D(\rho_{11}(\tau_m),\rho_b)=1$ at the time series τ_m. Notice that this parity condition does not fix the value of each $k_n^{\alpha\alpha}$ parameters but rather defines a large family of parameters values where the conditions $D(\rho_{00}(\tau_m),\rho_b)=0$ and $D(\rho_{11}(\tau_m),\rho_b)=1$ are verified. Furthermore, since the period τ is a scalable parameter in (18) and (17), the value of $\tau_m = \frac{\tau}{2} + m\tau$ can be scaled as desired.

Since the values of e and μ have been optimized for the $\alpha=\beta$ input configurations, the distances $D(\rho_{01}(t),\rho_b)$ and $D(\rho_{10}(t),\rho_b)$ driven by $\mathcal{H}_{01}$ and $\mathcal{H}_{10}$ for $\alpha \neq \beta$ are not *a priori* maximum at τ_m. To maximize those, the full series of the k_1^{00}, k_2^{00}, k_3^{00}, k_1^{11}, k_2^{11}, and k_3^{11} parameter obtained for $\alpha=\beta$ has been explored by a systematic combinatorial optimization process over more than 2-million combinations of the five, k_{00}^3 being arbitrary since it only controls $\langle\phi_e|\mathcal{H}_{00}|\phi_e\rangle$. We have taken benefit from our cyclic group approach to reduce

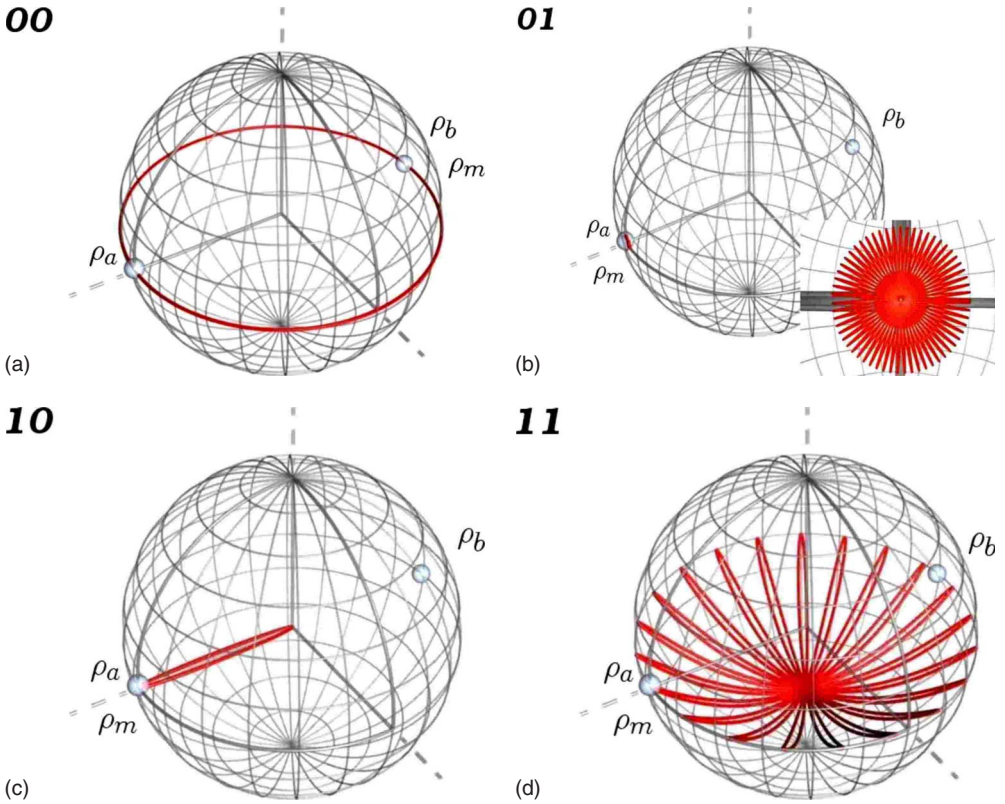

FIG. 2. (Color online) The $\rho(t)$ trajectories of the NOR gate plotted on the reduced Bloch sphere. ρ_a, ρ_b, and ρ_m are, respectively, the initial, the target, and the measured states. Only the $\{\alpha=0, \beta=0\}$ input configuration ρ_m reaches exactly ρ_b. In the three other cases ρ_m avoid ρ_b and as confirmed by the detailed $\rho_{01}(t)$ trajectory (see Fig. 1 inset), stays in this configuration near ρ_a. For those trajectories the structural parameters of the Hamiltonian are $\mu=e=0.033\ 67\ 17$ eV, while α and β take the value 0 or 1 eV, giving a $\tau=2\pi\times10^{-14}$ s period for the two $\rho_{00}(t)$ and $\rho_{11}(t)$ periodic trajectories.

the exploration to a set of five discrete parameters instead of a set of six continuous parameters if the optimization would concern directly the Hamiltonian. All the combinations of $k_n^{\alpha\alpha}$ parameters tested during the optimization process have been constrained to respect the $D(\rho_{00}(t),\rho_b)=0$ and $D(\rho_{11}(t),\rho_b)=1$ for the NOR gate. It appears that as long as $k_2^{11}<\min(|k_1^{11}|,|k_3^{11}|)$, the distance $D(\rho_{01}(t),\rho_b)$ remains high enough. In this case, it is sufficient to increase $|k_1^{11}|$ and $|k_3^{11}|$ to obtain a NOR gate fidelity close to 1. One inconvenient of this choice is that τ_m decreases a lot if the fidelity must remain larger than 0.9. Decreasing τ_m may lead to a measurement time too short as comparable to the available measurement instrument. One optimal set of parameter values is $\{k_{00}^1=2,\ k_{00}^2=3,\ k_{11}^1=25,\ k_{11}^2=5,\ k_{11}^3=-17\}$ which leads to a fidelity of $\mathcal{F}\approx0.99$. Increasing $|k_1^{11}|$ and $|k_3^{11}|$ again and the fidelity would reach unity but with a τ_m much lower than a femtosecond. Figure 2 presents the four trajectories of this optimized NOR gate plotted on the reduced Bloch sphere and respecting $D(\rho(\tau_m),\rho_b)=1-\alpha+\beta$.

For the $\{\alpha=1,\ \beta=1\}$ the maximum energy to run this NOR gate is $E=1.38$ eV for a trajectory oscillation period of $\tau=2\pi\times10^{-14}$ s. This is one order of magnitude higher than the quantum limit.

Notice that due to the asymmetry of our quantum system in Fig. 1, all the Boolean gates requiring $\mathfrak{B}(0,1)=1$ or $\mathfrak{B}(1,0)=1$ cannot be embodied in a QHC distance control approach because in this case, $D(\rho_{01}(t),\rho_b)$ and $D(\rho_{10}(t),\rho_b)$ are unable to reach one. Consequently, only the QHC distance controlled NOR, NXOR, and AND gates can be implanted with the Fig. 1 quantum system. The NXOR and AND gates have been successfully obtained using the method described above, only changing the parity conditions on the $k_i^{\alpha\alpha}$ parameters.

IV. DESIGN OF A NAND GATE IN A FREQUENCY CONTROL APPROACH

For the Hamiltonian (8) to drive a frequency controlled NAND logic gate in time, the $\rho(t)$ secular oscillation frequency Ω between the driving state ρ_a and the output target state ρ_b must verify $\Omega(\alpha,\beta)=k\alpha\cdot\beta$. Again, each (α,β) input defines one specific $\mathcal{H}_{\alpha,\beta}$ Hamiltonian and the consequent four Hamiltonians must (i) have the same structural parameters and (ii) the constant k in $\Omega(\alpha,\beta)=k\alpha\cdot\beta$ must only depend on the structural parameters e and μ. An efficient frequency controlled NAND logic gate can be designed by constructing a family of 3-states Hamiltonian (8) by expanding a 2-states $\mathcal{H}_{\text{eff}}$ whose secular oscillation frequency is verifying $\Omega(\alpha,\beta)=k\alpha\cdot\beta$. This expansion can be performed first for the $\alpha=\beta$ cases to avoid the spectral analysis of $\mathrm{Tr}[\rho(t)\rho_b]$ in search of a set of structural parameters leading to a secular frequency respecting the $\alpha\cdot\beta$ logic equation. After projection an Hamiltonian $\mathcal{H}$ leading to the effective Hamiltonian

$$\mathcal{H}_{\text{eff}} = \begin{pmatrix} 0 & \Omega/2 \\ \Omega/2 & 0 \end{pmatrix} \tag{20}$$

has three characteristic eigenvalues $-\frac{\Omega}{2}, \frac{\Omega}{2}$, and ξ where ξ is the eigenvalue associated to the less significant eigenvector. Driven by $\mathcal{H}$, $\text{Tr}[\rho(t)\rho_b]$ oscillates in time according to the superposition of three sinusoidal of frequencies $\omega_{12}=|\Omega|$, $\omega_{13}=|\frac{\Omega}{2}+\xi|$, and $\omega_{23}=|\frac{\Omega}{2}-\xi|$. Using again the $\mathcal{P}(\theta)$ rotation matrix introduced in Sec. III, the weight of each sinusoidal in $\text{Tr}[\rho(t)\rho_b]$ are $p_{\omega_{12}}=\frac{\cos^2(\theta)}{4}$, $p_{\omega_{13}}=\frac{\cos^2(\theta)\sin^2(\theta)}{4}$, and $p_{\omega_{23}}=\frac{\sin^2(\theta)}{4}$. The conditions for $\mathcal{H}$ to accept (20) as its effective Hamiltonian is therefore $p_{\omega_{12}}>p_{\omega_{23}}$ and $p_{\omega_{12}}>p_{\omega_{13}}$. Since $\forall\ \theta$, $p_{\omega_{12}}\geqslant p_{\omega_{13}}$, the only condition for ω_{12} to be the $\text{Tr}[\rho(t)\rho_b]$ secular frequency is $\theta\in[0;\frac{\pi}{4}[\cup]\frac{3\pi}{4};\pi]$. Respecting this condition, the most general form of a 3-states Hamiltonian leading to (20) is given by

$$\mathcal{H}(\theta) = \frac{1}{2}\begin{pmatrix} \sin^2(\theta)\left(\xi+\frac{\Omega}{2}\right) & \left(\xi-\frac{\Omega}{2}\right)-\cos^2(\theta)\left(\xi+\frac{\Omega}{2}\right) & \sqrt{2}\cos(\theta)\sin(\theta)\left(\xi+\frac{\Omega}{2}\right) \\ \left(\xi-\frac{\Omega}{2}\right)-\cos^2(\theta)\left(\xi+\frac{\Omega}{2}\right) & \sin^2(\theta)\left(\xi+\frac{\Omega}{2}\right) & \sqrt{2}\cos(\theta)\sin(\theta)\left(\xi+\frac{\Omega}{2}\right) \\ \sqrt{2}\cos(\theta)\sin(\theta)\left(\xi+\frac{\Omega}{2}\right) & \sqrt{2}\cos(\theta)\sin(\theta)\left(\xi+\frac{\Omega}{2}\right) & 2\xi\cos^2(\theta)-\frac{\Omega}{2}\sin^2(\theta) \end{pmatrix}. \tag{21}$$

The analytical form of the Hamiltonian $\mathcal{H}_{00}$ and $\mathcal{H}_{11}$, presenting, respectively, a secular frequency ω_{00} and ω_{11}, can be calculated using (21). For $\mathcal{H}_{00}$ where $\alpha=\beta=0$ and $\theta_{00}=0$, this leads to

$$\mathcal{H}_{00} = \begin{pmatrix} 0 & \frac{\omega_{00}}{2} & 0 \\ \frac{\omega_{00}}{2} & 0 & 0 \\ 0 & 0 & \xi \end{pmatrix}. \tag{22}$$

The Hamiltonian $\mathcal{H}_{11}$ can also be directly calculated using (21). However, this direct calculation leads to $\langle\phi_a|\mathcal{H}_{11}|\phi_a\rangle = \langle\phi_b|\mathcal{H}_{11}|\phi_b\rangle \neq 0$. Like in the case of the NOR gate, all the diagonal elements of $\mathcal{H}_{11}$ have been shifted to get $\langle\phi_a|\mathcal{H}_{11}|\phi_a\rangle = \langle\phi_b|\mathcal{H}_{11}|\phi_b\rangle = 0$, leading to

$$\mathcal{H}_{11}(\theta) = -\frac{1}{2}\begin{pmatrix} 0 & \left(\xi-\frac{\omega_{11}}{2}\right)-\cos^2(\theta)\left(\xi+\frac{\omega_{11}}{2}\right) & \kappa(\xi,\omega_{11},\theta) \\ \left(\xi-\frac{\omega_{11}}{2}\right)-\cos^2(\theta)\left(\xi+\frac{\omega_{11}}{2}\right) & 0 & \kappa(\xi,\omega_{11},\theta) \\ \kappa(\xi,\omega_{11},\theta) & \kappa(\xi,\omega_{11},\theta) & f(\xi,\omega_{11},\theta) \end{pmatrix} \tag{23}$$

with $f(\xi,\omega_{11},\theta)=2\xi\cos^2(\theta)-\sin^2(\theta)(\xi+\omega_{11})$ and $\kappa(\xi,\omega_{11},\theta)=\sqrt{2}\cos(\theta)\sin(\theta)(\xi+\frac{\omega_{11}}{2})$. Since the evolution driven by $\mathcal{H}_{00}$ belongs only to the subspace generated by $|\phi_a\rangle$ and $|\phi_b\rangle$, a shift of $\langle\phi_e|\mathcal{H}_{00}|\phi_e\rangle$ does not affect this evolution. The only structural parameters which must be compatible in the two Hamiltonians is therefore μ. Identifying the two μ values leads to

$$\omega_{00} = \xi - \frac{\omega_{11}}{2} - \cos^2(\theta)\left(\xi+\frac{\omega_{11}}{2}\right). \tag{24}$$

The solution of this equation gives the compatibility condition between $\mathcal{H}_{00}$ and $\mathcal{H}_{11}$,

$$\xi = \omega_{00}\left(\frac{1}{\sin^2(\theta)} + \frac{R}{2}\frac{1+\cos^2(\theta)}{\sin^2(\theta)}\right) \tag{25}$$

with $R=\frac{\omega_{11}}{\omega_{00}}$. With this ξ, $\mathcal{H}_{00}$ and $\mathcal{H}_{11}$ will have the same structural parameters, and $\mathcal{H}(\alpha,\beta)$ will be properly defined by normalizing its matrix elements using $\kappa(\xi,\omega_{11},\theta)$. To finalize our NAND gate, two conditions are required, $\omega_{11}=0$ and $\omega_{01}=\omega_{10}=\omega_{00}$. The first condition, characteristics of a NAND gate, leads to $R=0$ in (25), which gives the normalized structural parameters

$$e = \frac{\sqrt{2}}{\tan(\theta)} - \frac{\tan(\theta)}{\sqrt{2}} \tag{26}$$

and

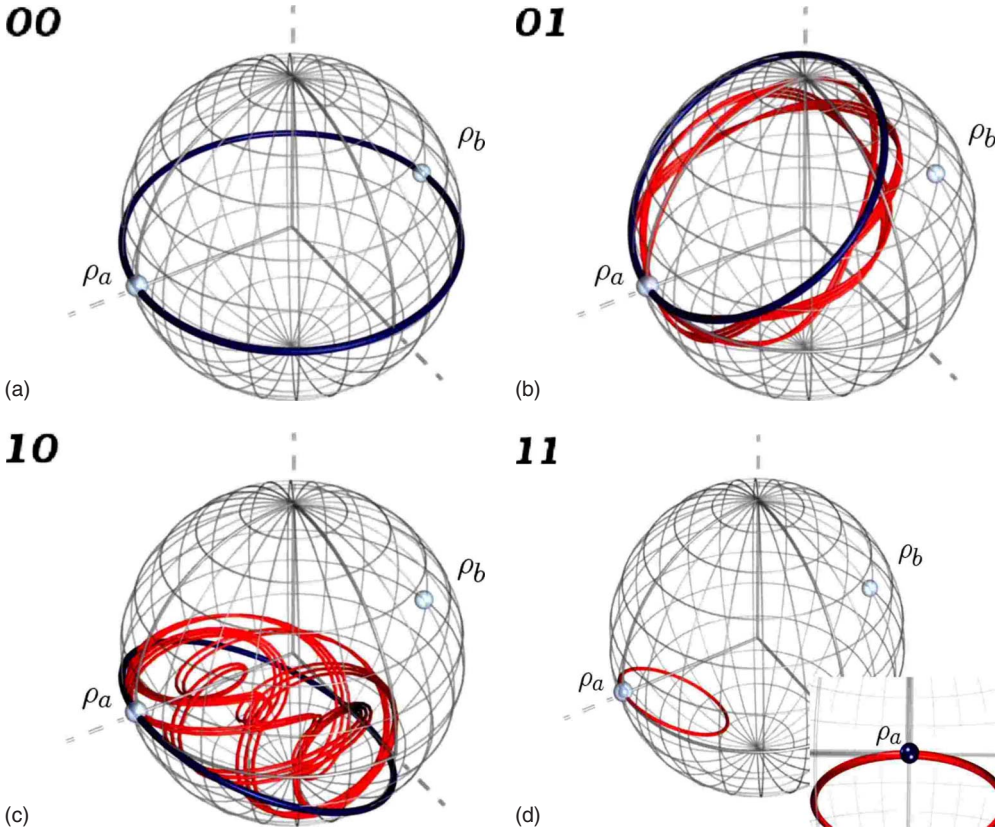

FIG. 3. (Color online) The $\rho(t)$ trajectories [grey (red)] and the trajectories driven by the effective Hamiltonian [black (blue)], both plotted, for one pseudoperiod, in each input configuration of the NAND gate, on the reduced Bloch sphere. ρ_a and ρ_b are, respectively, the initial and the target states. The secular frequencies of the $\{\alpha=0,\ \beta=0\}$, $\{\alpha=0,\ \beta=1\}$, and $\{\alpha=1,\beta=0\}$ input configurations are equal: $w_{00}=w_{01}=w_{10}=\frac{1}{4}$ PHz. For the $\{\alpha=1,\ \beta=1\}$ input configuration, even if the dominant frequency is $w_{11}=0$ Hz, the two other frequencies generate a residual oscillation of weak amplitude. Nevertheless, the effective trajectory stays at ρ_a and would reach ρ_b only for an infinite time (see Fig. 1 inset). The structural parameters of the Hamiltonian are $\mu=0.518\,485\,4$ eV and $e=1.410\,209\,4$ eV, while α and β take the value 0 or 1 eV. Notice that $\rho_{01}(t)$ and $\rho_{10}(t)$ never pass by ρ_b. But what is important here is not the distance between $\rho(t)$ and the target state but how long $\rho(t)$ will take to be at a minimum distance from ρ_b.

$$\mu = \frac{\tan(\theta)}{\sqrt{2}}. \tag{27}$$

To respect the second condition $\omega_{01}=\omega_{10}=\omega_{00}$, the optimum θ value, $\theta_{\text{opt}} \simeq \frac{723\pi}{3590}$ has been found by an optimization process. For this particular θ value, the fidelity of the gate given by (7) is exactly $\mathcal{F}=1$.

For the 11 input configuration, the secular frequency of (6) is $\Omega_-=\frac{e+3\mu}{2}-\frac{\Omega_0}{2}$. The e and μ values found in (26) and (27), with $\theta \in [0;\frac{\pi}{4}[\cup]\frac{3\pi}{4};\pi]$, lead to $\Omega_-=0$. The method developed here is equivalent to a $\text{Tr}[\rho(t)\rho_b]$ Fourier analysis looking for the e and μ values where the dominant component in the $\text{Tr}[\rho(t)\rho_b]$ Fourier spectrum is zero only for the 11-input configuration. The e and μ values leading to the Fig. 3 trajectories are one optimum to get a ideal frequency control NAND gate that is $\Omega(\alpha,\beta)=k\alpha.\beta$ using a minimum of three quantum states. The energy to run the Fig. 3 NAND is maximum for the $\{\alpha=0,\ \beta=1\}$ input and equals to $E=0.76$ eV for a frequency oscillation around one PHz.

Due to the impossibility to cancel out Ω_{01} and Ω_{10}, the Boolean function requiring $\mathfrak{B}(0,1)=0$ or $\mathfrak{B}(1,0)=0$ cannot be encoded with the system in Fig. 1. Consequently, aside the NAND gate presented here, only the XOR and OR gates can be designed in the QHC frequency control approach.

V. STABILITY OF THE NOR AND NAND GATE

The NOR and NAND gates constructed above suppose a complete separation between the corresponding 3-states quantum system and the environment. In this case, the quantum trajectory is very much periodic for the NOR and almost periodic for the NAND. There was no decoherence or fluctuations considered nor internally (not enough quantum states) nor externally. When now those 3-states quantum systems are not in perfect insulation from the environment, the corresponding interactions modify the $\rho(t)$ optimized trajectories and reduce the fidelity of the gate. It turns out that this trajectory perturbation can be reproduced statistically by perturbing the $\mathcal{H}(\alpha,\beta)$ matrix elements by a random part $\mathcal{N}$ leading to [20]

$$\mathcal{H}_p(\alpha,\beta) = \mathcal{H}(\alpha,\beta) + \eta\mathcal{N} \tag{28}$$

with η a scaling parameter. Because only a commutative perturbation can be studied analytically, we have first calcu-

lated how the above NOR and NAND gate trajectories are modified by a $\mathcal{N}$ respecting $[\mathcal{H}_0,\mathcal{N}]=0$ and with all its matrix elements randomly selected on the $[-\pi;\pi]$ interval. Since the elements of $\mathcal{N}$ are supposed to be dimensionless quantities, η has the dimension of an energy.

For a distance controlled gate, $\mathrm{Tr}[\rho(\tau_m)\rho_b]$ calculated using this perturbed Hamiltonian is exactly given by

$$\mathrm{Tr}[\rho(\tau_m)\rho_b] = \sum_{n=1}^{N} c_n^2 i_n^2 + 2m\sum_{n=1}^{N-1}\sum_{m=n+1}^{N} c_n c_m i_n i_m \cos[(\lambda_n-\lambda_m)\tau_m + \eta(s_n-s_m)\tau_m], \tag{29}$$

where the s_n are the $\mathcal{N}$ eigenvalues. The $\mathrm{Tr}[\rho(\tau_m)\rho_b]$ expected value is given by

$$\mathfrak{E}\{\mathrm{Tr}[\rho(\tau_m),\rho_b]\} = \frac{1}{(2\pi)^N}\int_{-\pi}^{\pi} ds_1 \int_{-\pi}^{\pi} ds_2 \cdots \int_{-\pi}^{\pi} ds_N \sum_{n=1}^{N} c_n^2 i_n^2 + 2\sum_{n=1}^{N-1}\sum_{m=n+1}^{N} c_n c_m i_n i_m \cos[(\lambda_n-\lambda_m)\tau_m + \eta(s_n-s_m)\tau_m] \tag{30}$$

the direct integration leads to

$$\mathfrak{E}(\mathrm{Tr}[\rho(\tau_m)\rho_b]) = K + 2\,\mathrm{sinc}^2(\pi\eta\tau_m)Q \tag{31}$$

with

$$K=\sum_{n=1}^{N} c_n^2 i_n^2 \quad \text{and} \quad Q=\sum_{n=1}^{N-1}\sum_{m=n+1}^{N} c_n c_m i_n i_m \cos[(\lambda_n-\lambda_m)\tau_m]. \tag{32}$$

Now, in the case of a frequency control and with still $[\mathcal{H}_0,\mathcal{N}]=0$, the perturbation $\mathcal{N}$ only changes the eigenvalues of the Hamiltonian without changing its eigenvectors. As a consequence, the weight $p_{\omega_{ij}}$ of each frequency in $\mathrm{Tr}(\rho(t)\rho_b)$ does not change with η. Therefore, the secular oscillation frequency $\Omega(\eta)$ is given by the same eigenvalues doublet. The secular unperturbed oscillation frequency $\Omega_0=|\lambda_i-\lambda_j|$ becomes

$$\Omega(\eta) = |(\lambda_i+\eta s_i)-(\lambda_j+\eta s_j)| \tag{33}$$

and the $\Omega(\eta)$ expected value is given by

$$\mathfrak{E}[\Omega(\eta)] = \frac{1}{(2\pi)^N}\int_{-\pi}^{\pi} ds_1 \int_{-\pi}^{\pi} ds_2 \cdots \int ds_N |(\lambda_i+\eta s_i) - (\lambda_j+\eta s_j)| = \frac{1}{(2\pi)^2}\int_{-\pi}^{\pi} ds_i \int_{-\pi}^{\pi} ds_j |(\lambda_i-\lambda_j)+\eta(s_i-s_j)| \tag{34}$$

the direct integration leads this time to

$$\mathfrak{E}[\Omega(\eta)] = \Omega_0 + \frac{1}{(2\pi)^2} H(2\pi\eta-\Omega_0)\left(\frac{1}{3\eta^2}(2\eta\pi-\Omega_0)^3\right), \tag{35}$$

where $H(x)$ is the Heavyside step function.

The two functions (31) and (35) represent the deviation of, respectively, a distance and a secular oscillation rate from their ideal values when a commutative noise source perturbs the system. They are consequently independent of any logic gate implementation, and are able to determine which type of control is less sensitive to this noise source.

The function (31) starts rapidly to deviate from its unperturbed value, to reach its limit, given by K, at $\eta=\frac{\hbar}{\pi\tau_m}$. This value of η is about 10^{-2} eV for a period of a few femtoseconds and K range between 0 and 1/2 since the initial and target states are orthogonal.

The function (35) starts to deviate from its initial value, Ω_0, when $\eta \geqslant \frac{\hbar\Omega_0}{2\pi}$, which range between 10^{-1} eV and 10^{-4} eV, for Ω_0, respectively, in the range of the PHz or the THz. This deviation is much slower than in the rate control case, since the asymptote of (35) is $\frac{2}{3}\pi\eta$.

For the two control solutions to be equivalently stable, the measuring time τ_m of the distance controlled trajectory must be small enough to ensure that $\frac{\hbar}{\pi\tau_m} \gg \frac{\hbar\Omega_0}{2\pi}$ leading to $\tau_m \ll (\frac{\Omega_0}{2})^{-1}$. With this fast distance control trajectory, two problems arise: (i) The time interval to perform the measure would be around 10^{-4} fs, way beyond the expected time resolution of a measuring instrument. (ii) The energy required to run this very fast evolution would be much higher than the energy required in the rate control case, and the two gates would not be comparable.

Consequently, let us consider a distance and frequency controlled gates, requiring the same amount of energy and running with a fidelity equal to 1. Perturbing those two gates with a noise source, the distances reached at τ_m by the distance controlled gate deviate faster and in a more critical way from their unperturbed values than the dominant oscillation frequencies of the trajectories of the frequency controlled gate. This leads to a better immunity of the rate controlled implementation toward a noise source respecting $[\mathcal{H}_0,\mathcal{N}]=0$ whatever the logic gate considered. As an example, the fidelities of the distance controlled NOR and rate controlled NAND gates, designed in Secs. II and III, are shown in Fig. 4. Those fidelities are computed with (7), substituting each $\mathcal{M}_{\alpha\beta}$ by the corresponding $\mathfrak{E}\{\mathrm{Tr}[\rho_{\alpha\beta}(\tau_m)\rho_b]\}$ or $\mathfrak{E}(\Omega_{\alpha\beta}(\eta))$ for, respectively, the NOR and NAND gate. This figure confirms the robustness of the rate controlled NAND gate toward the noise source intensity η, since for $\eta=0.1$ eV, the fidelity of the gate remains superior to 0.7. The fidelity of distance controlled NOR gate falls quickly to its minimum of 0.05, for $\eta=0.02$ eV, and remains around this value for greater values of η.

This result may appear biased because the secular oscillation frequency Ω is less affected by a commutative noise than $\mathrm{Tr}[\rho(t),\rho_b]$ since the weight of the frequencies are not modified. Therefore, to confirm the noise immunity of the frequency controlled NAND gate, the fidelity of the two gates, in the presence of a more general random perturbation of (8), has been computed numerically. For this purpose, the effect of two different noncommutative noise sources had been studied: An $\mathcal{N}_{\mathrm{diag}}$ perturbation in (36) affecting only the diagonal terms of $\mathcal{H}(\alpha,\beta)$ and an $\mathcal{N}_{\text{off-diag}}$ perturbation affecting only its off-diagonal terms, the $\mathcal{N}_{\mathrm{diag}}$ and $\mathcal{N}_{\text{off-diag}}$ matrix elements being randomly and uniformly distributed on the

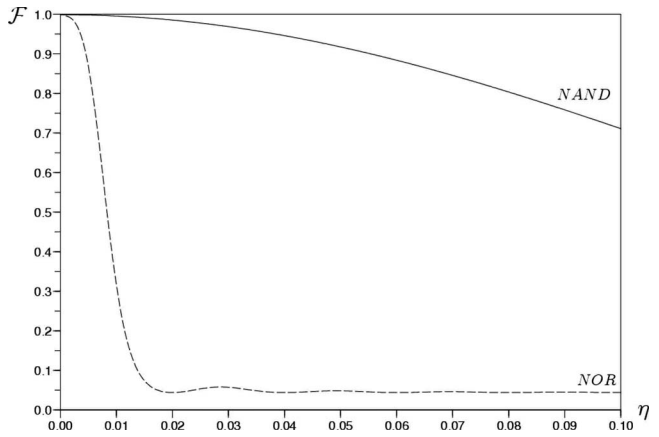

FIG. 4. Analytical fidelities of the NAND and NOR gates using a commutative noise source as a function of the scaling parameter η (eV). The NAND rate controlled gate is less sensitive to this noise source than the NOR distance controlled gate. For $\eta=0.02$ eV the fidelity of the NOR distance controlled gate reaches its minimum whereas the fidelity of the NAND gate remains high enough reaching its minimum for a much higher value of η.

$[-\pi;\pi]$ interval. The a and b scaling parameters of those two noises were tuned to create a two-dimensional fidelity landscape with the perturbed Hamiltonian given by

$$\mathcal{H}_p(\alpha,\beta) = \mathcal{H}(\alpha,\beta) + a\mathcal{N}_{\text{diag}} + b\mathcal{N}_{\text{off-diag}}. \tag{36}$$

The results of this numerical exploration, led over 1000 $\mathcal{N}_{\text{diag}}$ and $\mathcal{N}_{\text{off-diag}}$ for each value of a and b, are presented in Fig. 5 for both NOR and NAND gates. It confirms that a NAND frequency controlled gate is more stable than a NOR distance controlled gate. For the frequency controlled NAND gate and with large a and b values, the fidelity of the gate remains better than 0.7. On the contrary, for a distance controlled NOR gate, the fidelity falls down very quickly to zero, except for a perfectly diagonal noise in (36). Indeed a distance controlled NOR gate is more sensitive to off-diagonal perturbations than a frequency controlled NAND gate which in turn is more sensitive to a diagonal noise.

VI. CONCLUSION

In the framework of the quantum Hamiltonian computing approach where a classical logic gate is implemented using a quantum system, we have constructed very simple NOR and NAND logic gates with three quantum states. To build the gate Hamiltonian matrix elements, a distance and a frequency control approach of the system quantum trajectory have been, respectively, used. After a very sharp optimization, both approaches are leading to very performant gates. In a distance controlled approach and aside from the NOR gate presented here, very efficient AND and NXOR gates can also be optimized using three quantum states. In a frequency control approach and aside from the NAND gate presented here, XOR and OR gates can be produced. The stability study of those QHC implementations shows that the distance control approach is very sensitive to external fluctuations in its Hamiltonian. Such a gate must be perfectly isolated from the environment to ensure a fully periodic trajectory. On the other hand, a frequency control approach does not impose such a strong constraint on the trajectory and is therefore less sensitive to fluctuations in its Hamiltonian structure. Since its

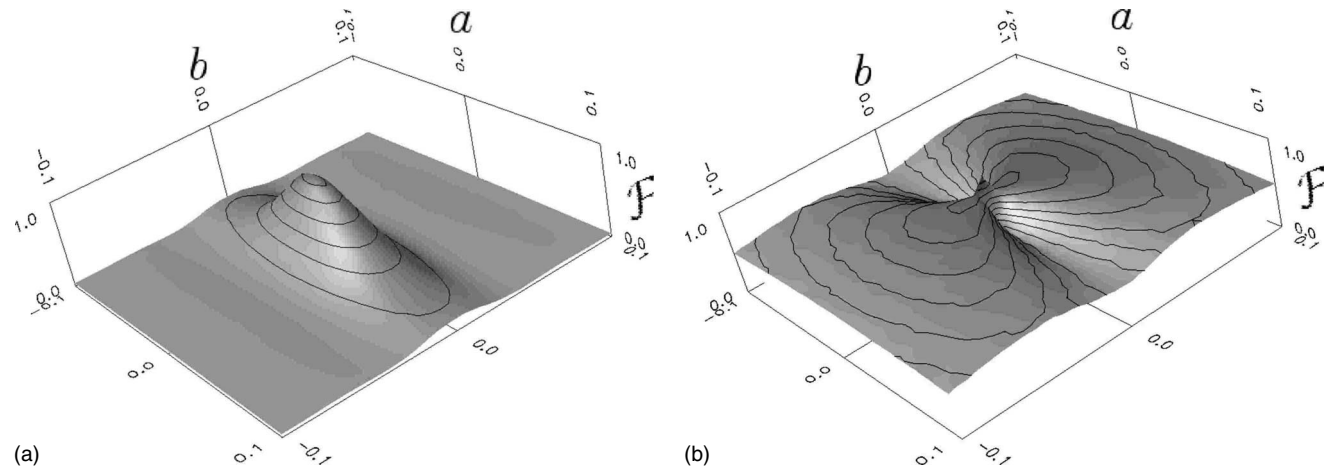

FIG. 5. Fidelity of the NOR (1) and NAND (2) gates as a function of the scaling parameters a and b (eV) of two random Hamiltonians, one diagonal and the other off diagonal. The scaling parameters, a and b, of the two noise sources goes from −0.01 eV up to 0.5 eV. At each (a,b) point, the fidelity of the system has been computed over 1000 different random Hamiltonians. The fidelity of the NOR distance controlled gate in the off-diagonal perturbation direction decreases extremely quickly reaching almost zero for an amplitude of 0.05 eV. In general the distance controlled NOR gate is very sensitive to the noise. The fidelity is acceptable in only a small region around the unperturbed Hamiltonian. On the contrary, the rate controlled NAND gate presents a large region where the fidelity is acceptable. In the direction where the fidelity is the most sensitive, that is the diagonal perturbation part, the fidelity decreases slowly to reach 0.7 for a noise amplitude of ± 0.1 eV.

running secular frequency is directly related to the tunneling current intensity passing through the gate when the gate is interacting with metallic electrodes, this frequency control offers an easy way to access the logic gate output as compared with a distance controlled gate. For more complex QHC gates and in view of the extremely sharp tuning required with a distance control design, only the frequency control approach is now being explored further searching for Hamiltonians whose eigenvalues fulfilled the awaited Boolean equation while changing well identified elements of its matrix.

ACKNOWLEDGMENT

We thank the EU Commission for its financial support through the ICT PICO-INSIDE integrated project.

[1] A. M. Nielsen and I. L. Chuang, *Quantum Computation and Quantum Information* (Cambridge University Press, Cambridge, 2000).
[2] J. Fiurasek, N. Cerf, I. Duchemin, and C. Joachim, Physica E (Amsterdam) **24**, 161 (2004).
[3] F. Remacle and R. D. Levine, Phys. Rev. A **73**, 033820 (2006).
[4] C. Joachim, J. Phys.: Condens. Matter **18**, S1935 (2006).
[5] R. P. Feynman, Optics News **11**, 11 (1985).
[6] D. Deutsch, Proc. R. Soc. London, Ser. A **400**, 97 (1985).
[7] C. Joachim, I. Duchemin, J. Fiurasek, and N. J. Cerf, Int. J. Nanosci. **4**, 107 (2005).
[8] I. Duchemin and C. Joachim, Chem. Phys. Lett. **406**, 167 (2005).
[9] I. Duchemin, N. Renaud, and C. Joachim, Chem. Phys. Lett. **452**, 269 (2008).
[10] C. Joachim and M. Ratner, Proc. Natl. Acad. Sci. U.S.A. **102**, 8801 (2005).
[11] U. Fano, Rev. Mod. Phys. **29**, 74 (1957).
[12] J. Samuel, Pramana, J. Phys. **47**, 361 (1996).
[13] F. Bloch, Phys. Rev. **70**, 460 (1946).
[14] R. Siroski, *Boolean Algebra* (Springer-Verlag, Berlin, 1964).
[15] See EPAPS Document No. E-PLRAAN-78-194811 for a demonstration of those technical points. For more information on EPAPS, see http://www.aip.org/pubservs/epaps.html.
[16] M. Tinkham, *Group Theory and Quantum Mechanics* (McGrawHill, New York, 1964).
[17] I. N. Herstein, *Abstract Algebra* (Wiley, New York, 1996).
[18] C. Joachim, Chem. Phys. **116**, 339 (1987).
[19] D. Maynau, Ph.D. thesis, Universite Paul Sabatier, 1987.
[20] W. Fischer, H. Leschke, and P. Mueller, Ann. Phys. **7**, 59 (1998).